

INVESTIGATING AVALANCHE INTERACTION WITH DEFENCE STRUCTURES USING UNMANNED AERIAL SYSTEM PHOTOGRAMMETRY

Marc S. Adams^{1*}, Jan-Thomas Fischer¹, Andreas Kofler¹, Christian Tollinger², Armin Graf¹, Johannes Hoffmann³ and Reinhard Fromm¹

¹ Department of Natural Hazards, Austrian Research Centre for Forests (BFW), Innsbruck, Austria

² Austrian Service for Torrent and Avalanche Control (WLV), Innsbruck, Austria

³ Whiteroom Productions, Innsbruck, Austria

ABSTRACT: Unmanned aerial system photogrammetry (UAS-P) is increasingly becoming a commonplace tool to generate orthophotos and measure surface elevation with ground sampling distances in the centimetre-range. In this contribution, we present results from a UAS-P mission to map an avalanche event, which occurred near the city Innsbruck in Western Austria. The main objective of the campaign was to document avalanche extent and volume, as well as investigate avalanche interaction with different types of defence structures, located in the track and runout area. The results of this case study showed that in total, 70.000 m³ of snow and debris were deposited. The highest deposition depths (> 5 m) were reached where a rocky outcrop reduced the width of the track from 40 to 15 m, and near the deposition terminus, where the avalanche impacted several concrete wedges, catching and deflection dams. A comparison between slope angles and deposition depths showed, that the main part of the deposition volume originated from medium deposition depths (2.1-2.2 m) at slope angles between 15-25°, which covered ~62% of the total deposition area. The combination of orthophoto interpretation and spatial deposition analysis revealed that terrain variations such as channelisation and defence structures locally dominate the deposition pattern. Knowledge of these local effects is of major importance to understand the interaction of avalanches with defence structures and improve their design.

KEYWORDS: Snow depth distribution, mitigation measures, unmanned aerial vehicle

1. INTRODUCTION

Mapping the extent and depth of avalanche deposition along the avalanche track and in the runout zone is a crucial step in event documentation (Fuchs et al., 2007). It provides important input to process understanding (Kofler et al., 2018), evaluating defence structure effectiveness (Margreth and Romang, 2010), as well as testing and enhancing avalanche simulations (Fischer et al., 2015; Teich et al., 2014). The proliferation of unmanned aerial system photogrammetry (UAS-P) has made an easy-to-use mapping tool readily available, which can be flexibly deployed to generate orthophotos and measure surface elevation with ground sampling distances (GSD) in the centimetre-range (Colomina and Molina, 2014; Nex and Remondino, 2013).

On January 21, 2018, an avalanche event occurred in the Arzler Alm catchment, above the city Innsbruck in Western Austria. The release area was located between 1,940 and 2,240 m

a.s.l. (mean inclination: 41°, total size: 8.6 hectares). The avalanche split into three separate tracks, before merging above a glacial terrace (1,050 m a.s.l.), where the runout zone was located. As avalanches originating in the Arzler Alm catchment have in the past reached the outskirts of Innsbruck and caused damage there, extensive mitigation measures were put in place. Therefore the terrain in the runout zone has been heavily altered by the construction of several generations of defence structures, including braking mounds (i.e. concrete wedges and earth cones), as well as deflection and catching dams. These measures have proven very effective here, especially with regard to retarding wet snow avalanches (Hopf and Neuner, 1975). In this contribution, we present an application of UAS-based mapping of the afore-mentioned avalanche event, as a basis for studying avalanche's interaction with the defence structures in the runout zone.

* Corresponding author address:

Marc S. Adams, Department of Natural Hazards,
Austrian Research Centre for Forests (BFW)
6020 Innsbruck, Austria
tel: +43 (0)512 573933 5177
email: marc.adams@bfw.gv.at

2. METHODS

We mapped the deposition in the lower section of the avalanche track and the runout zone (target area size: 0.6 km²) using a custom-built fixed-wing UAS (Multiplex Mentor, wingspan 1.6 m), fitted with an off-the-shelf digital camera (Sony NEX5, 14MP). For a detailed description of the UAS setup, the reader is referred to Adams et al. (2018). 1,200 aerial images were recorded on January 24, 2018 from approximately 140 m a.g.l. and photogrammetrically processed using structure-from-motion software (Agisoft Photoscan, v1.4).

The resulting orthophoto (GSD: 0.04 m) was used to delineate the extent of the avalanche deposition and construe additional information regarding avalanche granule sizes and flow behaviour. The photogrammetric point cloud (density: 40 points/m³) representing surface heights, was georeferenced with eight ground control points and classified into snow and non-snow (mostly vegetation and artificial surfaces). The latter were deleted, the point cloud clipped to the area of interest and gaps filled by linear interpolation. The deposition amount was then calculated based on snow-off terrain heights (DTM) recorded in 2009 during an airborne laser scanning (ALS) campaign (AdTLR, 2010). Both deposition thickness (slope perpendicular) and depth (plumb line) were derived directly from the point clouds in geographic information software (SAGA LIS Pro 3D, v 3.0.7). Additionally, in-situ measurements of deposition depths were performed with snow probes along three transects in the central part of the runout zone. Probe locations were recorded with a Garmin GPSMAP 64s (typical accuracy: 3 m at 1 σ).

3. RESULTS AND DISCUSSION

3.1 *Deposition outline and volume*

The deposition area has a size of approximately 50 x 610 m (3 hectares; red polygon in Figure 1a/b). A gravel road (at 1,190 m a.s.l.) defines its upper boundary, above which the main avalanche track widens from 10 to 40 m and two of the three above-mentioned tracks join. The upper-most mitigation measure (a concrete wedge) is located 80 m below the road in the centre of the track. At 1,120 m a steep rocky outcrop (>60° inclination) on the orographic right creates a bottleneck, narrowing the track to a width of 15-20 m. In this section, the track is for the most part laterally constrained by steep (>35°), forested slopes. Below the narrow point, the avalanche crosses two gravel roads (at 1,070 and 1,040 m a.s.l.); the terrain flattens slightly (from 20-25° to 15-20°) and opens into a large basin. Here the avalanche runs out into the central section of defence structures, consisting of wedges, as well as catching and deflections dams, which are located below the lower gravel road (Figure 1a). The DTM indicates a

multitude of additional defence structures in this area, which are not described here, as they did not influence the described event.

The deposition depth varies strongly within the observed area: A first small local maximum is located near the single wedge in the upper track section, where snow depths of 3-5 m are reached. A majority of deposition was recorded in the bottleneck section, where depths of >5 m were measured. Further downstream, small accumulations can be observed in front of the concrete wedges in the central runout area. The avalanche was eventually stopped by a series of deflection and catching dams in the lower runout, where maximum deposition depths of up to 11 m were reached. In total, approximately 70,000 m³ of snow and debris were deposited, resulting in a mean deposition depth of 2.4 m (Fig 1b). These findings are in good agreement with the results of the back-calculation of this event with the computational avalanche simulation tool SamosAT, presented in a related publication (Kofler et al., 2018).

Interpreting the results, several aspects were considered to check their validity and accuracy:

- i) Local snow depth prior of the event was unknown, but could be inferred from the undisturbed snow pack in the runout to be within 0.5-1 m (Figure 1b). The lateral and lower boundaries of the deposition area were derived from mapping the border between the undisturbed snow pack and the avalanche. As the avalanche may have covered undisturbed snow in the runout, rather than entraining it, the deposition volume should be considered a maximum value.
- ii) The upper deposition boundary was chosen rather arbitrarily, mainly based on the location of the deposition maximum below and signs of snow erosion / entrainment above the upper gravel road (Figure 4). Shifting this boundary would however result in a change of deposition volume.
- iii) The catchment is not systematically monitored, therefore previous small-scale events may have contributed to the recorded total volume of the observed event.
- iv) Errors in volume calculation may result from changes of the snow-off terrain heights since they were recorded in 2009. This becomes apparent in the area on the orographic right of the avalanche terminus, where negative deposition depths were recorded (Figure 1b). However, a spot check of the ALS DTM showed that only small areas show terrain changes > 0.2 m during this period.
- v) Although the deposition area is steep (mean slope angle: 21°), the difference in volume between deposition depth and thickness is only approximately 5% of the total deposition volume in favour of the former.

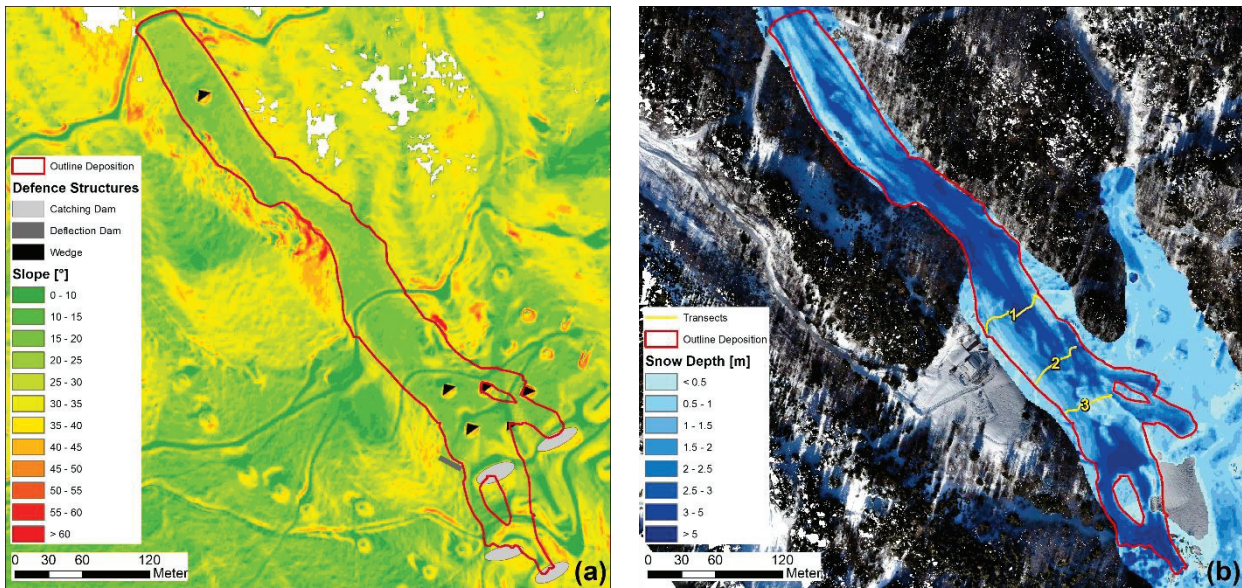


Figure 1: Slope [°] in the deposition area, derived from ALS DTM with symbols indicating type and location of defence structures (dams and wedges), which have an impact on the deposition, outline of deposit (red polygon) (a); snow depth [m] and location of transects (yellow lines) with IDs, against UAS-orthophoto (b).

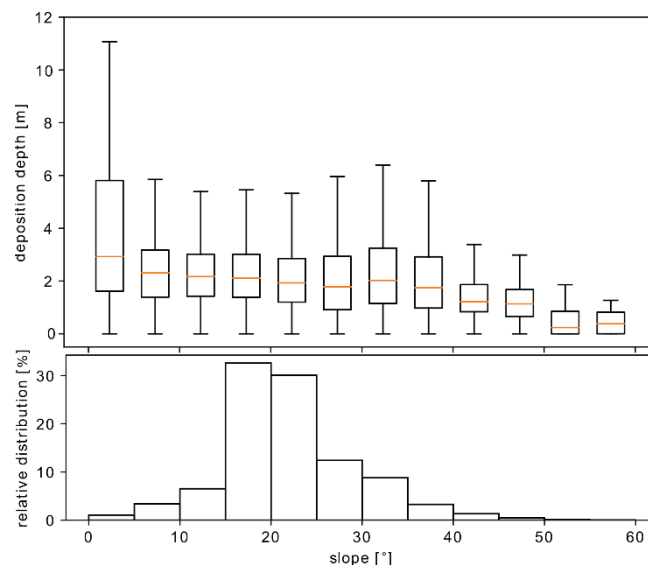


Figure 2: Distribution of deposition depth [m] ($d = h * \cos \theta$) and relative (area) distribution in runout area with respect to slope [°], derived from ALS DTM.

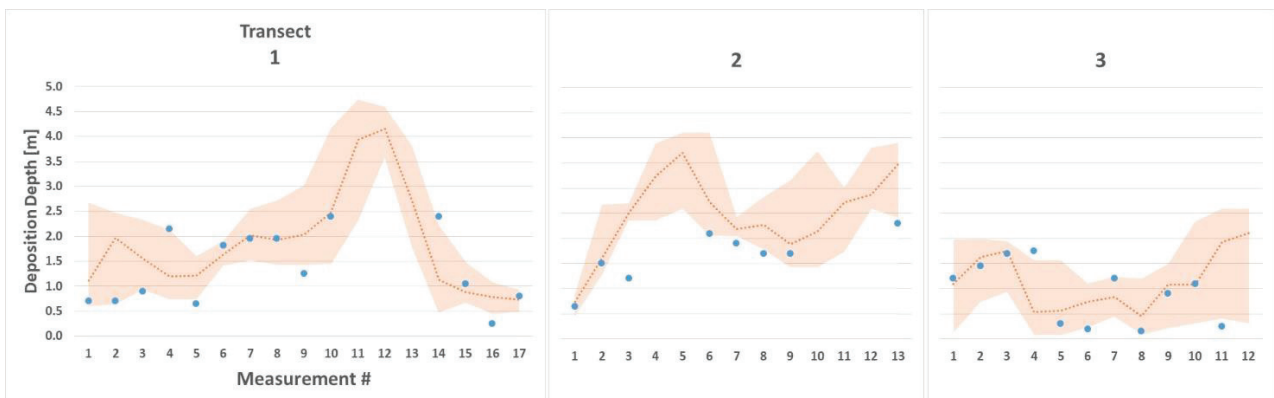


Figure 3: Comparison of in-situ (blue dots) and UAS snow depth measurements (orange) within a 3 m radius around the in-situ measurement point (dashed line – mean; area – min / max) at all three transects (Fig.1b).

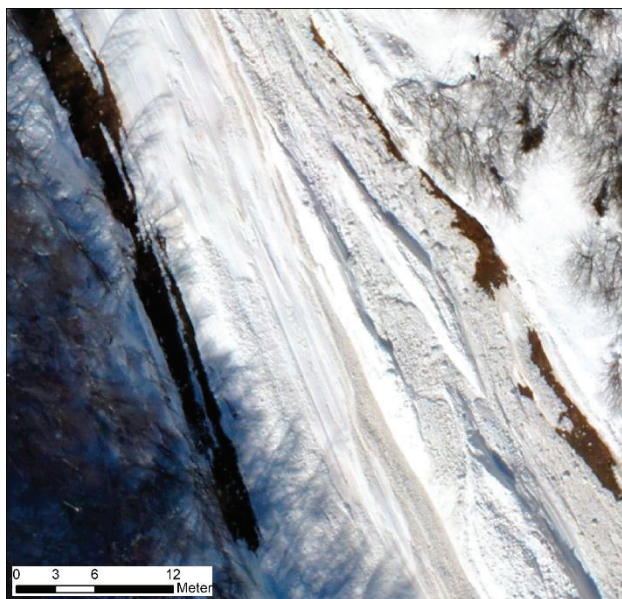


Figure 4: Signs of snow erosion / entrainment in the avalanche track above the upper boundary of the deposition area (extract from UAS orthophoto).

3.2 Deposition depth vs slope

The distribution of deposition depths in relation to the slope angle shows the deposit depth is generally negatively correlated with the slope angle (Figure 2). This is in correspondence to observations from other test sites (Sovilla et al., 2010) and means that on steep slopes, the deposit is shallow and on gentle slopes, the deposit is deep.

Besides the negative correlation between deposition depth and slope, the depth distribution of the Arzler Alm avalanche shows another distinct feature. There are two local maxima in the distribution of deposition depth as shown in Figure 2: The highest mean deposition (3.8 m) on areas with 0-5° inclination and a peak (2.3 m) on areas with 30-35°, which is the typical slope angle of the terrain in front of the catching dams in the runout.

Here it is important to note, that although the highest deposition depths are observed for low slope angles below 5° they only account for a small fraction of the total volume, since these areas only cover ~1% of the runout zone. The main part of the deposition volume originates from medium deposition depths (2.1-2.2 m) at slope angles between 15-25°, which cover ~62% of the total area. For slope angles between 25 and 40° (which cover ~23% of the area with deposition depth ~2 m) a steep drop in deposition depth was observed; above 50° inclination, no considerable deposition occurs.

3.3 Comparison of transect with UAS snow depth measurements

The in-situ measurements of the snow depth are in reasonable agreement with the UAS results, considering the high spatial variability of the deposition depth and a positional accuracy of the probe locations of 3 m (1σ) (Figure 3). Global error measures were calculated for all transect points: Root mean square error 0.76 m; mean average error 0.57 m. At some locations (e.g. points 11-13 in transect 1) snow depth exceeded the length of the probe, therefore no in-situ data could be recorded and only UAS snow depth was plotted in Figure 3.

4. CONCLUSION AND OUTLOOK

In this contribution, we used UAS-P to map volume and extent of a recent avalanche event. This data served as a basis for analysing the interaction between the avalanche and defence structures in the runout. The combination of orthophoto interpretation and spatial deposition analysis showed that terrain variations such as channelisation and defence structures locally dominate the deposition pattern. Knowledge of these local effects is of major importance to understand the interaction of avalanches with defence structures and improve their design. This contribution highlights the benefits of operational close-range sensing for avalanche research.

Work leading on from this contribution will exploit the very high-resolution UAS-based orthophotos, surface and terrain elevation measurements to further study small-scale deposition patterns, granule size and distribution as well as flow behaviour of avalanches around defence structures (Figure 5).

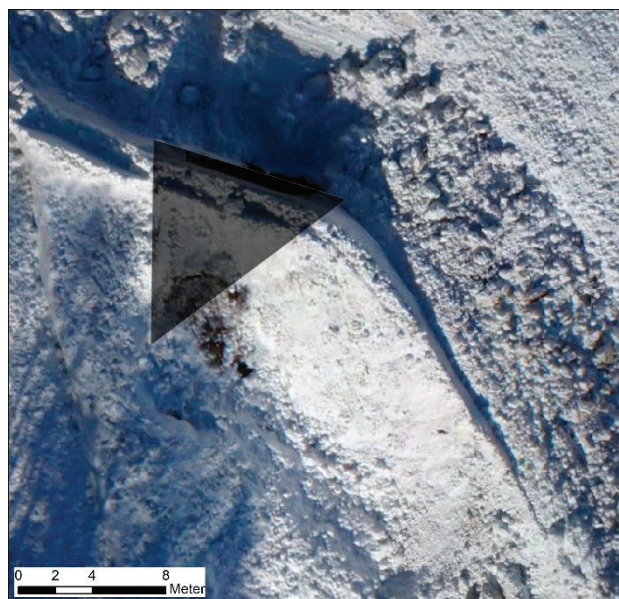


Figure 5: Close-up from the UAS orthophoto, showing avalanche flow behaviour when impacting a concrete wedge in the runout (black triangle).

ACKNOWLEDGEMENTS

The authors would like to express their sincere gratitude to Natalie Brozova and Klaus Suntinger from the BFW for assisting the fieldwork and TIRIS (AdTLR) for supplying the ALS DTM.

REFERENCES

- Adams, M.S., Bühler, Y. and R. Fromm, 2017: Multitemporal accuracy and precision assessment of unmanned aerial system photogrammetry for slope-scale snow depth maps in alpine terrain. *Pure and Applied Geophysics*, DOI: <https://doi.org/10.1007/s00024-017-1748-y> (in print).
- AdTLR (Amt der Tiroler Landesregierung), 2010: Landesweite Laserscanbefliegung Tirol 2006-2010. Available online <https://www.tirol.gv.at/sicherheit/geoinformation/geodaten/laserscandaten> (last access: 21.08.2018).
- Colomina, I., and P. Molina, 2014: Unmanned aerial systems for photogrammetry and remote sensing: A review. *ISPRS Journal of Photogrammetry and Remote Sensing*, 92, 79–97.
- Fischer, J.-T., Kofler A., Fellin W., Granig M. and K. Kleemayr, 2015: Multivariate parameter optimization for computational snow avalanche simulation. *Journal of Glaciology*, 61(229), 875–888.
- Fuchs, S., Thöni M., McAlpin M.C., Gruber U. and M. Bründl, 2007: Avalanche hazard mitigation strategies assessed by cost effectiveness analyses and cost benefit analyses—Evidence from Davos, Switzerland. *Natural Hazards*, 41(1), 113–129.
- Hopf, J. and J. Neuner, 1975: Die Lawinenschutzmaßnahmen auf der Innsbrucker Nordkette, in: Hochwasser- und Lawinenschutz in Tirol. Land Tirol (Hg.), Interpraevent 1975, Innsbruck, pp. 205 – 214.
- Kofler, A.; Tollinger, C.; Jenner, A., Granig, M. and M. Adams, 2018: Braking mounds in avalanche simulations - a SamosAT case study International Snow Science Workshop, Innsbruck, Austria - 2018.
- Margreth, S. and S. Romang, 2010: Effectiveness of mitigation measures against natural hazards. *Cold Regions Science and Technology*, 64(2), 199–207.
- Nex, F., and F. Remondino, 2013: UAV for 3D mapping applications: A review. *Applied Geomatics*, 6(1), 1–15.
- Sovilla, B., McElwaine, J. N., Schaer, M. and J. Vallet, 2010: Variation of deposition depth with slope angle in snow avalanches: measurements from Vallée de la Sionne *Journal of Geophysical Research*, 115.
- Teich, M., Fischer J.-T., Feistl T., Bebi P., Christen M. and A. Grêt-Regamey, 2014: Computational snow avalanche simulation in forested terrain, *Nat. Hazards Earth System Sciences*, 14, 2233-2248.